Electronic Supplementary Material (ESI) for Journal of Materials Chemistry C.


# Using Ultra-Fast Spectroscopy to Probe the Excited State Dynamics of a Reported Highly Efficient Thermally Activated Delayed Fluorescence Chromophore.

Ricardo Javier Vázquez [a], Hyungjun Kim [b], Paul M. Zimmerman [a], and Theodore Goodson III [a,*]

[a] Department of Chemistry, University of Michigan, Ann Arbor, MI 48109

[b] Department of Chemistry, Incheon National University, Incheon 22012, Republic of Korea

* tgoodson@umich.edu

# Supporting Information

**Materials:** All the chromophores in this study were obtained from commercial suppliers and used without further purification. BCC-TPTA was purchased from Luminescence Technology Corporation and dissolved in toluene. The $Ir(BT)_2(acac)$ was purchased from Sigma and was dissolved in THF. And, the Rhodamine B was purchased from Sigma and dissolved in ethanol.

**Sample Preparation and Experimental Sample Handling:** A stock solution ($10^{-4}$ M) were prepared by mixing each sample in the corresponding solvent. Toluene, THF, and Ethanol were the solvent used for BCC-TPTA, $Ir(BT)_2(acac)$, and the Rhodamine B, respectively. Consequent dilutions from the stock solutions were made on each sample to run the different experiments conducted in this report. A 400 nm excitation wavelength were used in all experimental set-ups and for all the chromophores while their emissive lifetime were measured at their respective emissive $\lambda_{MAX}$. In all cases, including the temperature dependence measurements, emission quenching from purging oxygen is carried out. Specifically, the oxygen free atmosphere was created by bubbling $N_2$ thought the solution for at least 8 minutes. The 8 minutes criteria was based on the reproducibility of the emission spectrum and emissive lifetime characterization of the $Ir(BT)_2(acac)$ system. After 6 minutes on average, the emission intensity was at its higher counts for the $Ir(BT)_2(acac)$, meaning that oxygen was not quenching its triplet state.

**Quantum Yield Calculation:** The fluorescence quantum yields measurements were conducted by using the Williams comparative method. The optical density was measured to be ~ 0.10 or bellow to avoid reabsorption and internal filter effects. The absorption and fluorescence were measured for four samples with decreasing concentrations. The quantum yield was calculated using the following equation:

$$\phi_x = \phi_{STD} \frac{Grad_x \eta_x^2}{Grad_{STD}\, \eta_{STD}^2}$$

were $\Phi_x$ is the calculated quantum yield, $\eta$ is the refractive index of the solvent, and $Grad$ is the slope obtained from plotting the fluorescence area in function of the optical density (OD). The quantum yields for BCC-TPTA dissolved in toluene and for $Ir(BT)_2(acac)$ dissolved in THF were measured using Coumarin 30 ($\Phi = 0.67$)[1] dissolved in acetonitrile as the standard. The same is true for the $\Phi_x$ measurements after purging out oxygen (10 minutes). Rhodamine B is a well-known standard and the $\Phi$ value can be find elsewhere. The $\Phi$ of Rhodamine B after purging out oxygen (10 minutes) were measured as well and compared to itself ($\Phi$ = 0.67)[2] before purging. The emission spectra were collected on a Fluoromax-4 fluorimeter with slits set at 1 nm and an integration time of 0.100 s. Quartz cells with 10 mm path lengths were used for all the steady-state measurements. All optical measurements were carried out at STP.

**Stern-Volmer equation handling**: The emission of a chromophore can be quenched in the presence of a quencher, which is explained elsewhere.[3–5] The two main intermolecular process are responsible for this emission quenching are: quenching of the $S_1$ due to collisions between the chromophore and the quencher, or energy transfer from the $T_1$ state of the chromophore to the quencher. When the quencher is oxygen, energy transfer from the triplet of the chromophore to oxygen has been reported. The Stern-Volmer equation allow us to investigate the kinetics of these intermolecular quenching processes in function of the concentration of the quencher. For this analysis, the emissive lifetimes, before and after the quencher is added, are correlated with the ambient concentration of the oxygen in an equation expressed by:

$$\frac{t_o}{t} = 1 + K.t_o.[Q\}$$

In which the $t_o$ correspond to the chromophore lifetime before the quencher is added, the $t$ correspond to the chromophore lifetime after the quencher is added, the $K$ correspond to the quencher rate coefficient, and the $Q$ correspond to the quencher's concentration. It is well known that oxygen is an excellent triplet state quencher. Therefore, this equation was used in to understand the possible intermolecular quenching processes. The quencher rate constant is compared with the rate of diffusivities of the quencher to understand if the quencher can quench the chromophore via collision.

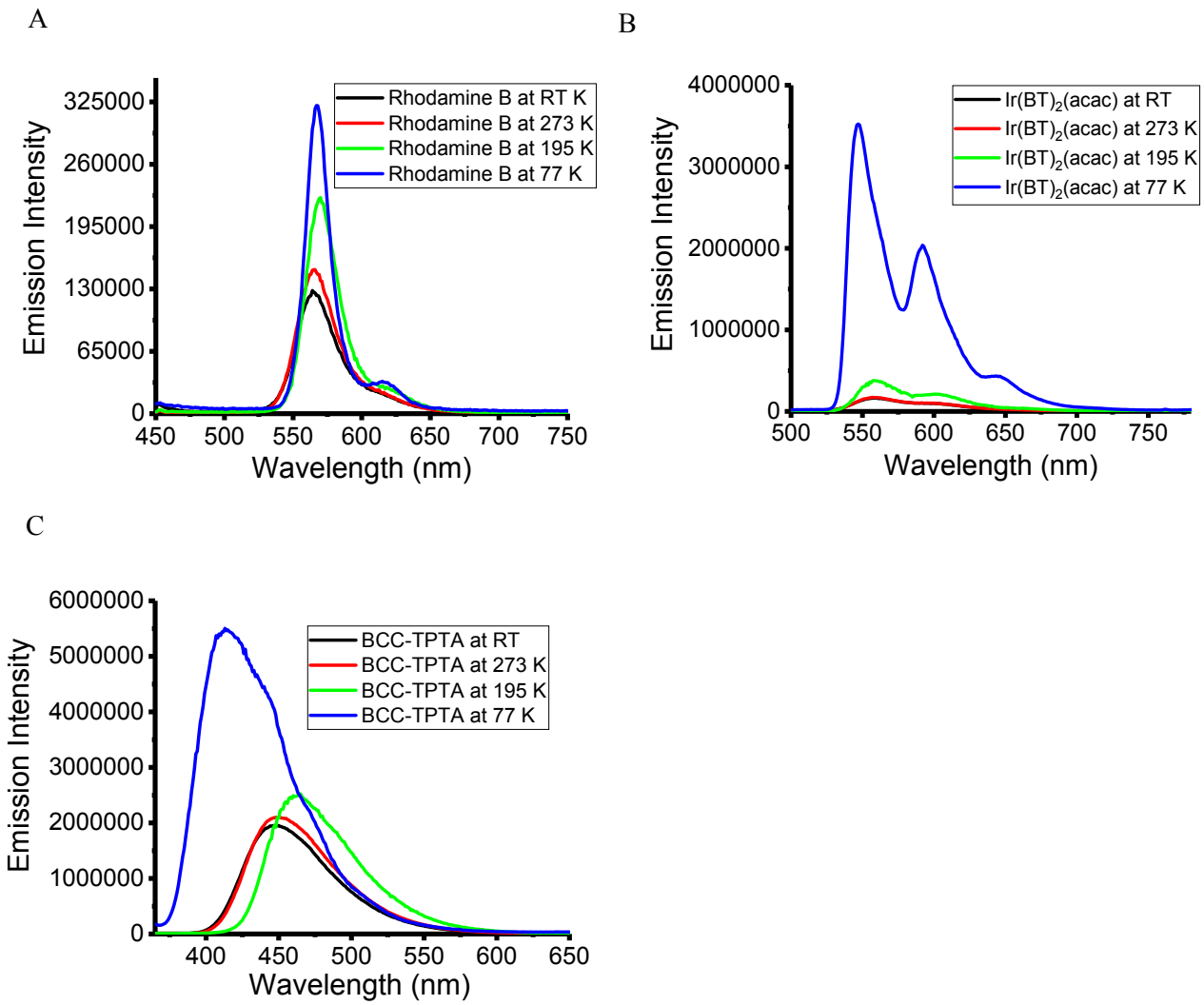


***Figure S1.*** Raw emission spectrum of the investigated chromophore at RT (black), 273 K (red), 195 K (green), and at 77K (blue): Rhodamine B (A), $Ir(BT)_2acac$ (B), and BCC-TPTA in toluene (C). No delayed between the excitation beam and the detection was done in these measurements. Also, these measurements were taken in oxygen free atmosphere after the samples were bubbled with $N_2$.

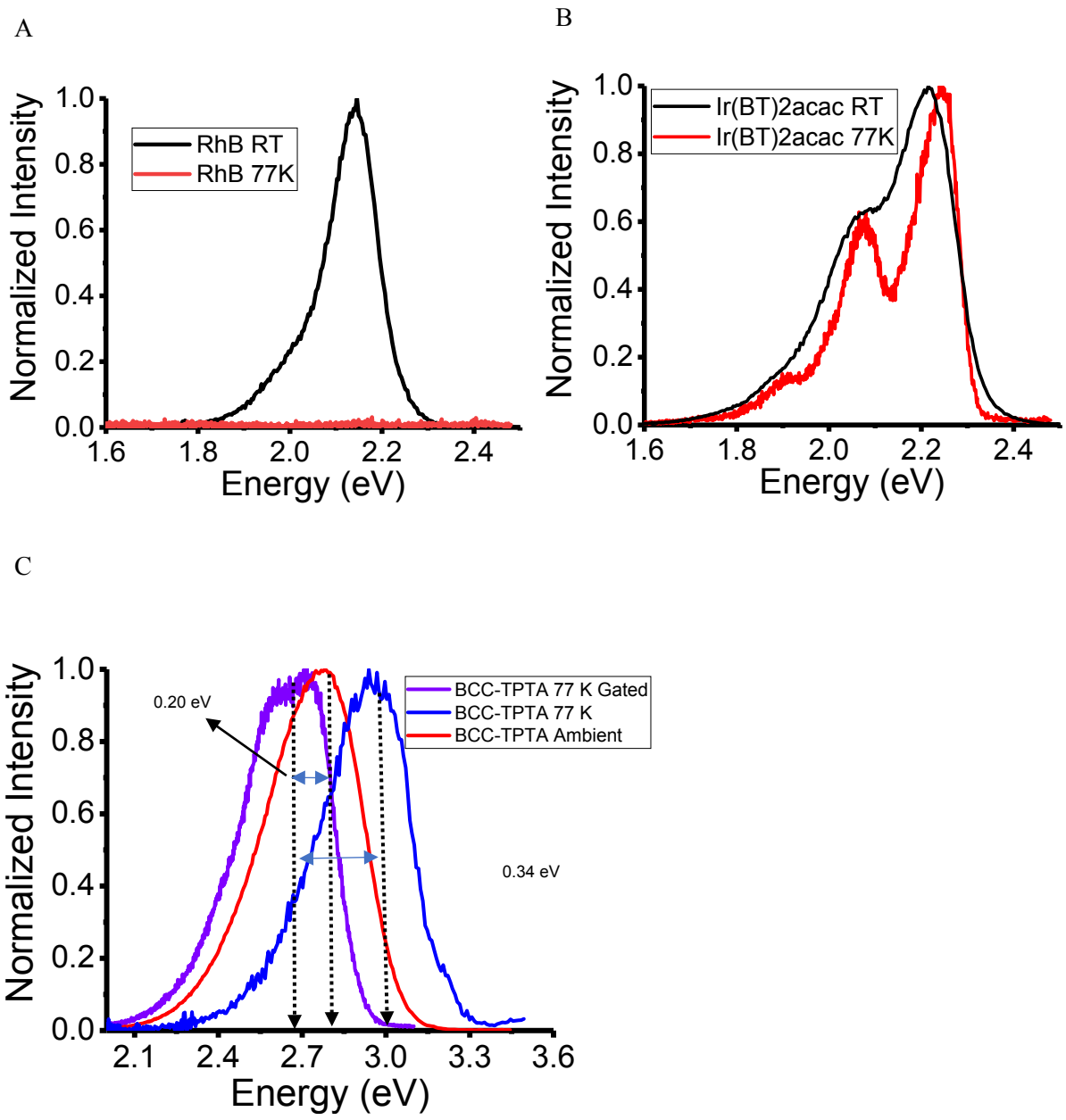


***Figure S2.*** Normalized emission spectrum of the investigated chromophore at RT and at 77K: Rhodamine B (A), $Ir(BT)_2(acac)$ (B), and BCC-TPTA (C). For BCC-TPTA, the emission spectrum at 77 K, 77 K gated (with a delayed > 150 μs between the excitation beam and the detected emission detection), and at RT was measured and compared. The delayed > 150 μs between the excitation beam and the emission detection was done with an electrical shutter to avoid the detection from the $S_1$ state at 77K.

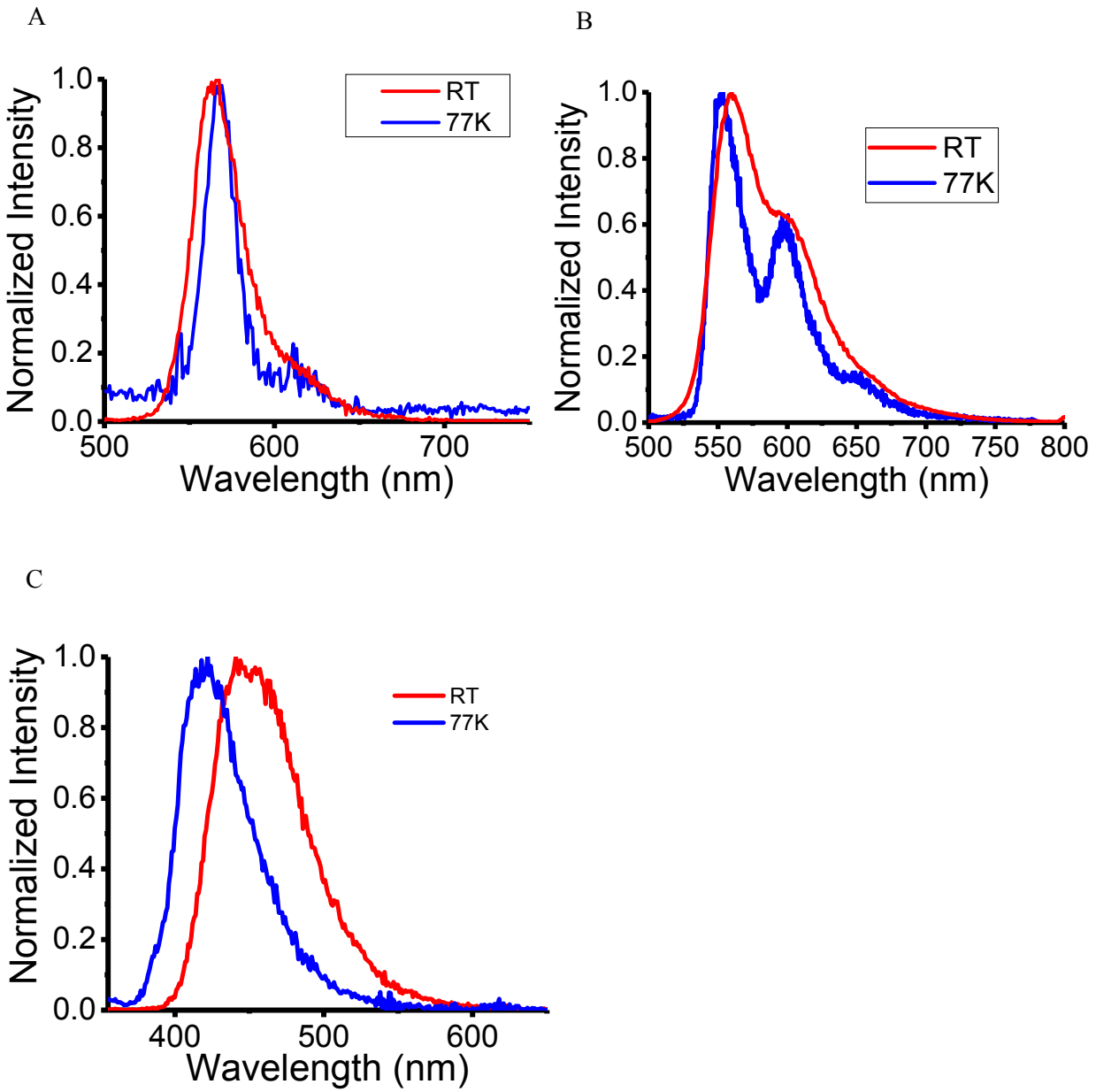


***Figure S3.*** Normalized emission spectrum of the investigated chromophore at RT and at 77K: Rhodamine B (A), $Ir(BT)_2acac$ (B), and BCC-TPTA (C). No delayed between the excitation beam and the detection was done in these measurements.

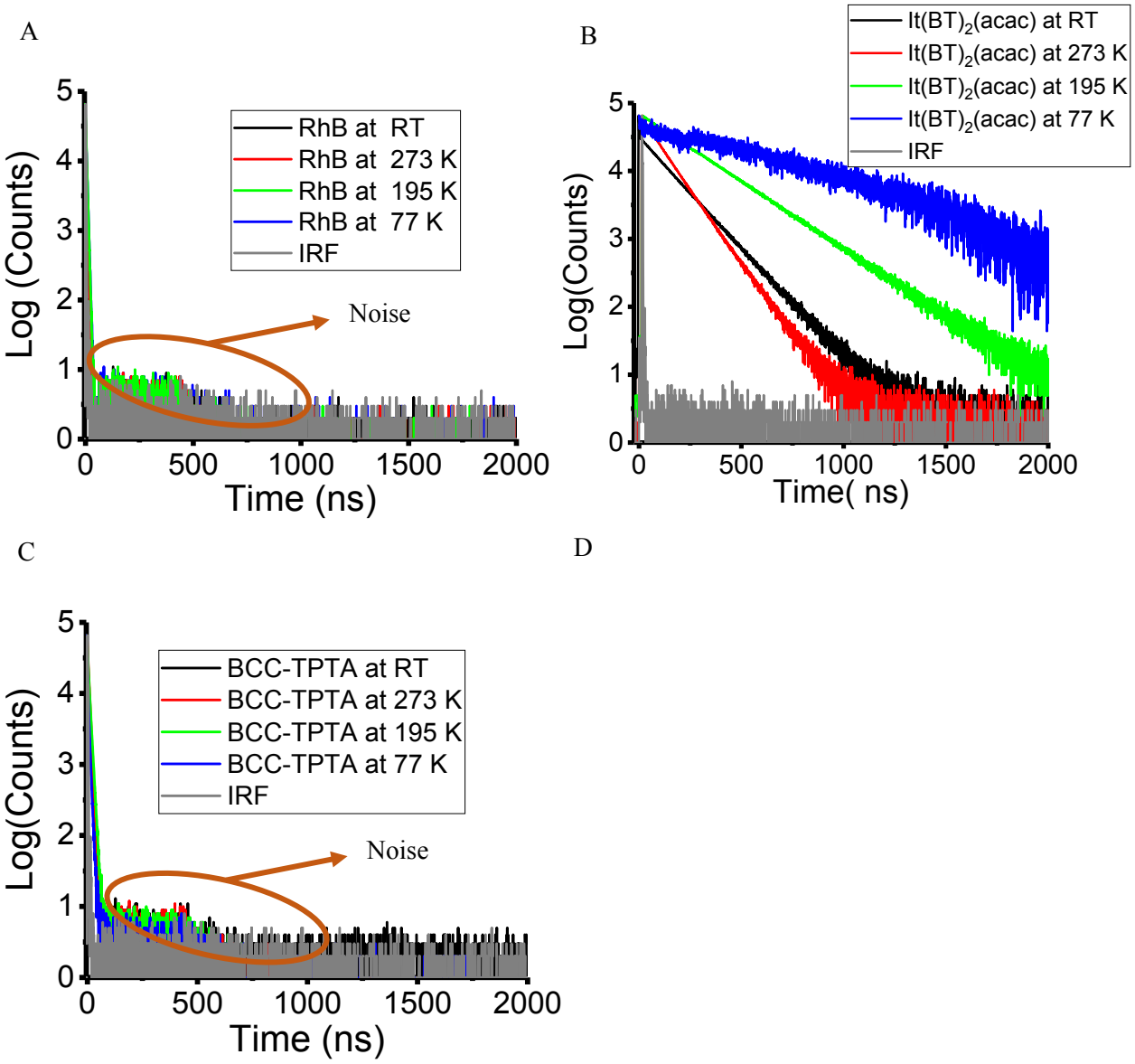


***Figure S4.*** Emissive lifetime characterization at different temperature obtained with the TCSPC technique. Rhodamine B was diluted in ethanol (A), $Ir(BT)_2(acac)$ in THF (B), and BCC-TPTA in toluene (C). Measurements were taken at the emission $\lambda_{max}$ obtained from ***Figure S3*** with a 400 nm excitation wavelength. Also, these measurements were taken in oxygen free atmosphere after the samples were bubbled with $N_2$.

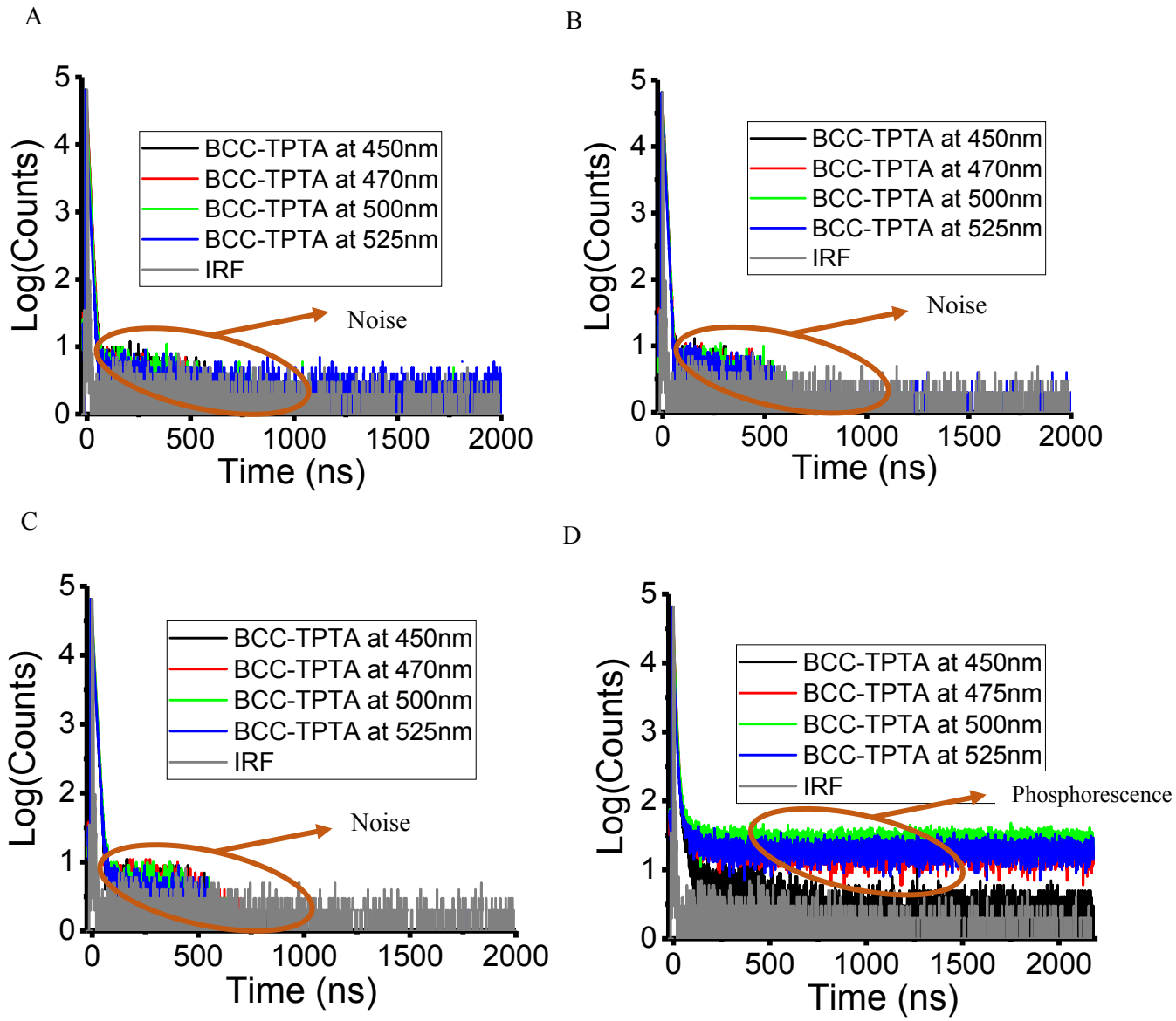


***Figure S5.*** Emissive lifetime characterization at different temperature and different detection wavelengths of BCC-TPTA obtained with the TCSPC technique. Measurements were taken in toluene solutions with a 400 nm excitation wavelength. RT (A), 273 K (B), 195 K (C), and 77 K (D). Also, these measurements were taken in oxygen free atmosphere after the samples were bubbled with $N_2$.

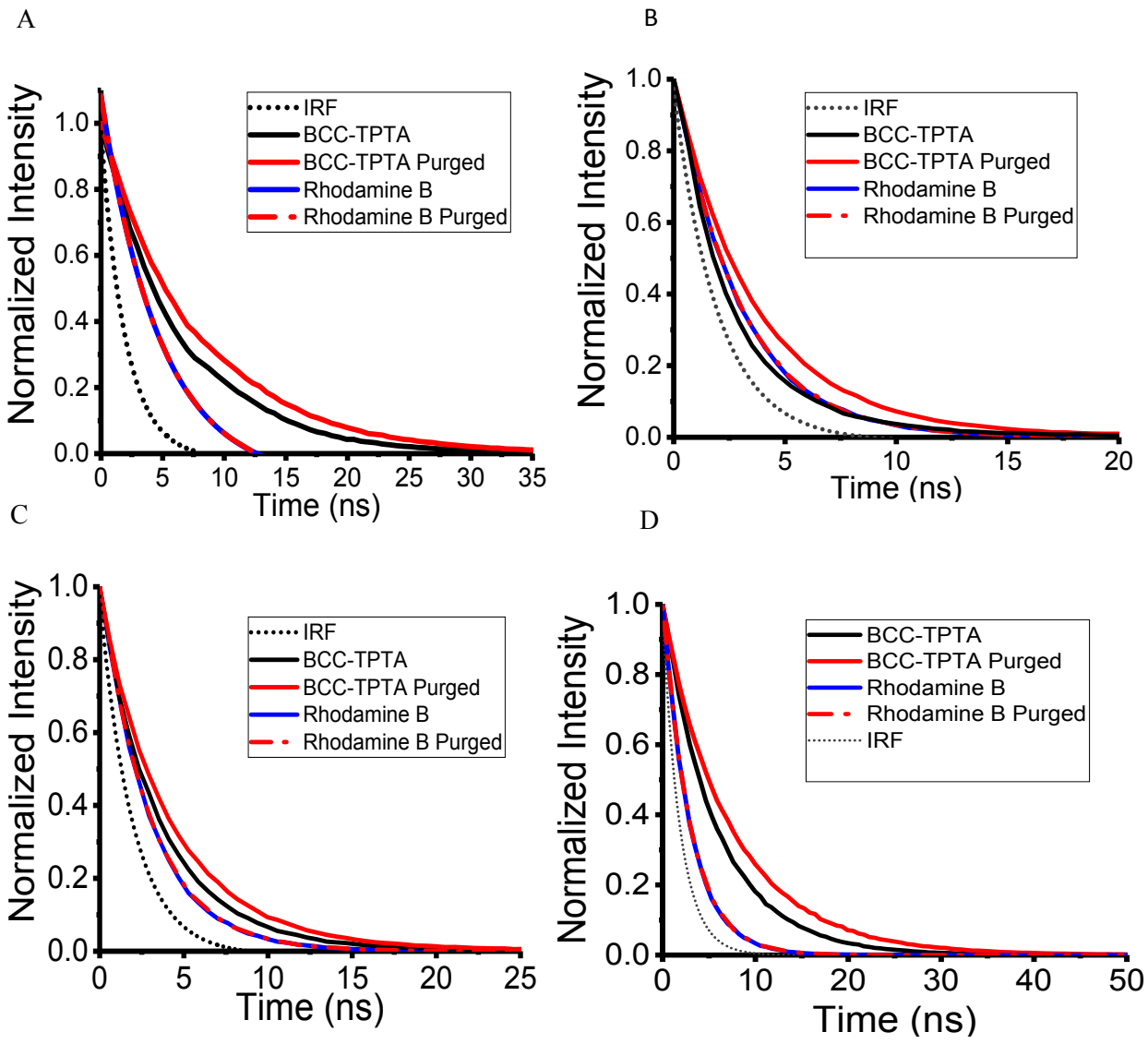


***Figure S6.*** The emissive lifetime of the chromophores was investigated by using Time Correlated Single Photon Counting (TCSPC) technique: BCC-TPTA in toluene (A), BCC-TPTA in hexane (B), BCC-TPTA in cyclohexane (C), and BCC-TPTA in chloroform (D). All of the Rhodamine B measurements were conducted in ethanol.

| Sample | Emissive lifetime | Emissive lifetime (Purged) |
|---|---|---|
| **Rhodamine B** | 2.97 ± 0.03 ns | 2.99 ± 0.04 ns |
| **BCC-TPTA in Hexane** | 2.69 ± 0.02 ns | 3.9 ± 0.1 ns |
| **BCC-TPTA in Cyclohexane** | 3.4 ± 0.1 ns | 4.2 ± 0.1 ns |
| **BCC-TPTA in Toluene** | 6.4 ns | 7.8 ns |
| **BCC-TPTA in Chloroform** | 10 ns | 13 ns |

***Table S1***. Fluorescence lifetime of BCC-TPTA in different solvents before and after the oxygen purging process. This measurements were done with the TCSPC technique.

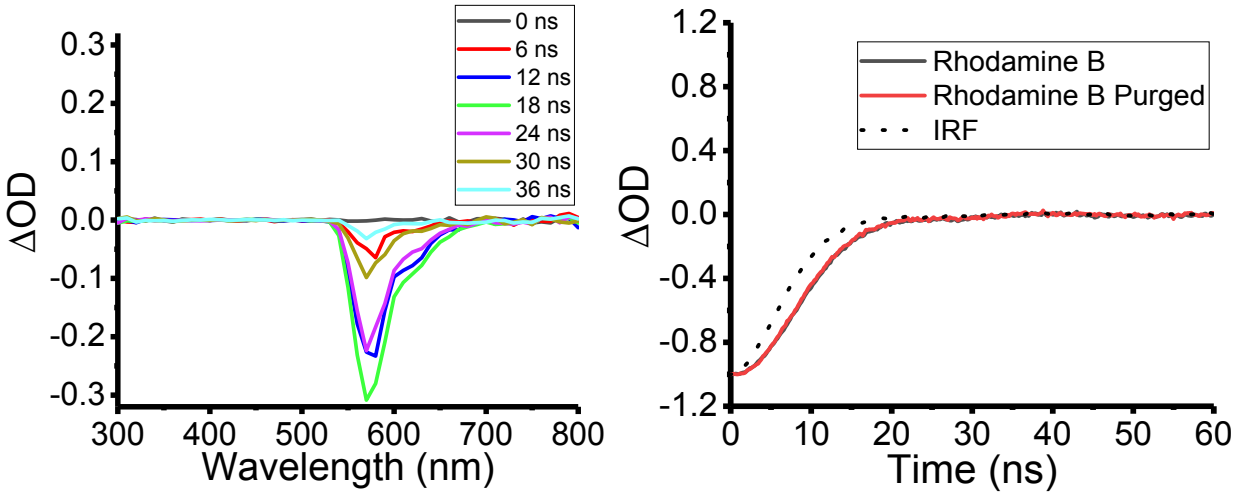


***Figure S7.*** Time-resolved absorption spectra of Rhodamine B after the oxygen purging process (A) and the kinetic trace of its time-resolved absorption spectrum bands before and after the oxygen purging process (B). Therefore, this band is attributed to the emissive relaxation process from the $S_1$ to $S_0$ (typical fluorescence).

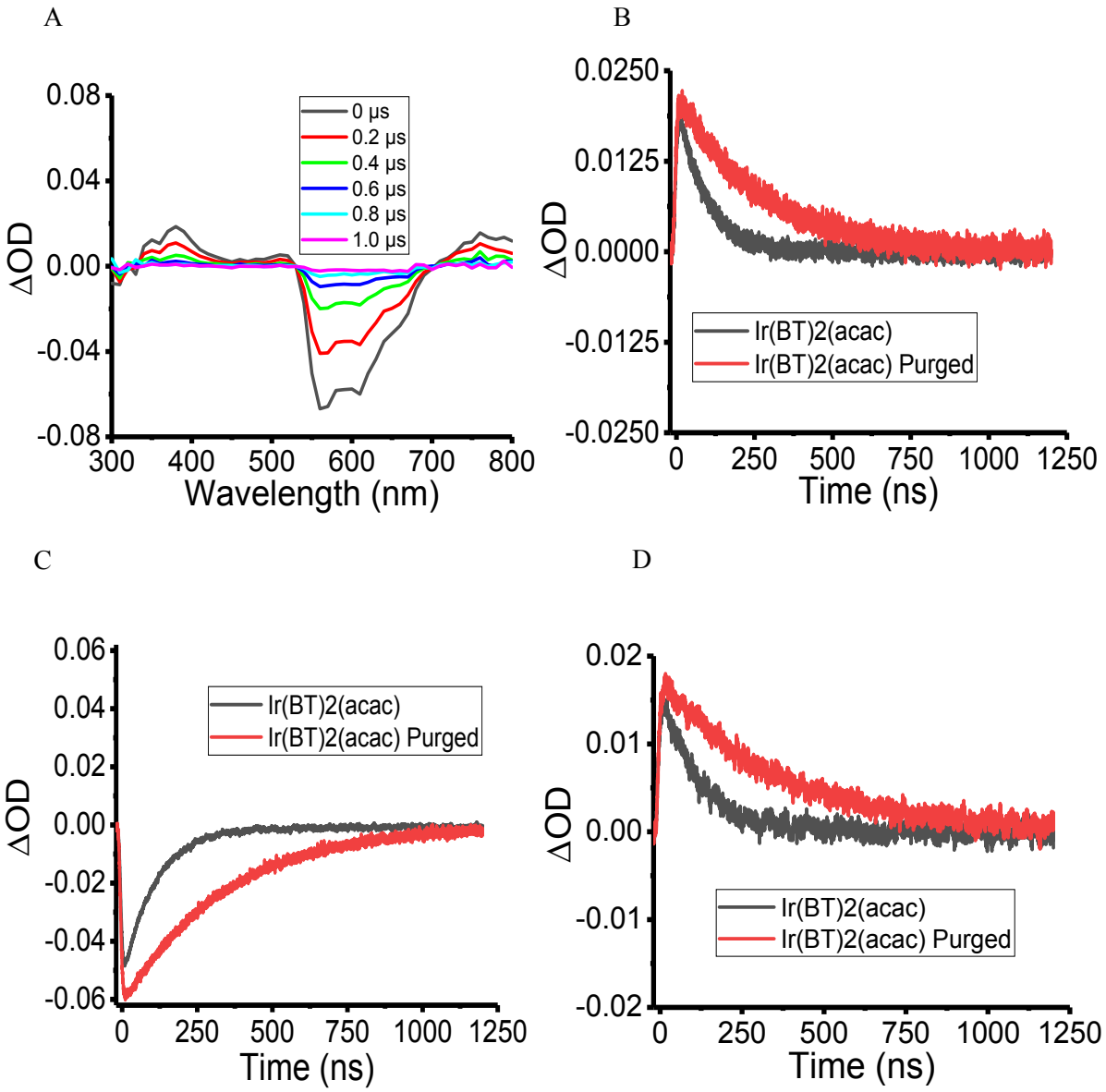


***Figure S8.*** Time-resolved absorption spectrum of the $Ir(BT)_2acac$ complex after the oxygen purging process (A). The kinetic traces of the 380 ns ESA (A), 565 nm SE (B), and 780 nm ESA (C) of $Ir(BT)_2(acac)$ before and after the oxygen purging process. As it can be observed, the time-resolved absorption spectrums is highly sensitive to the presence of oxygen.

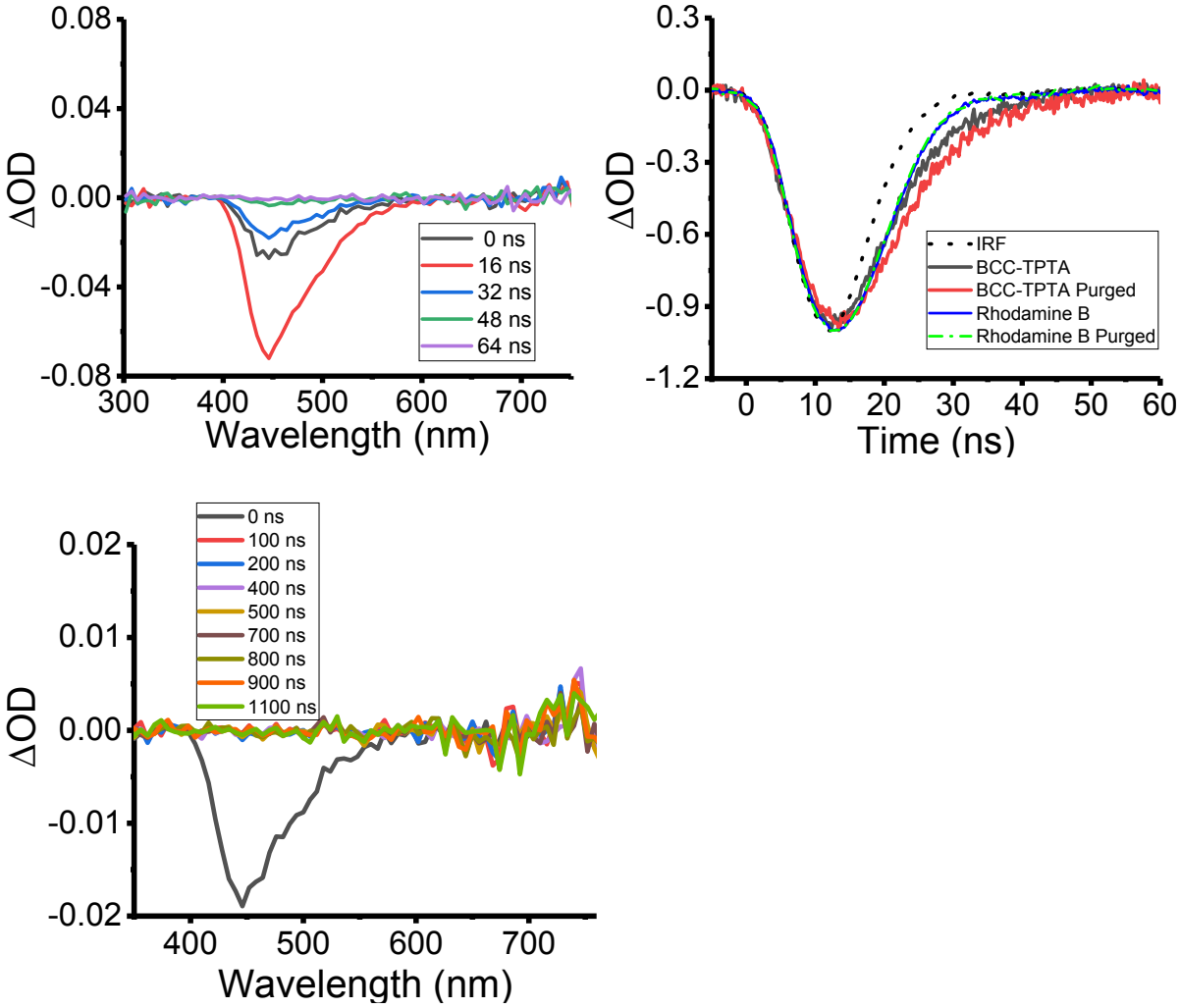


***Figure S9.*** Time-resolved absorption spectra of BCC-TPTA after the oxygen purging process. This time-resolved absorption band overlaps with the emission spectrum of BCC-TPTA (***Figure 1B***). Therefore, this band is be attributed to the emissive relaxation process from the $S_1$ to $S_0$ (typical fluorescence).

| Chromophore | Emissive Lifetime (TCSPC) | Emissive Lifetime Purged (TCSPC) | Negative OD Kinetic Trace (ns TAS) | Negative OD Kinetic Trace Purged (ns TAS) | ESA Kinetic Trace (ns TAS) | Purged Kinetic trace (ESA) ns TAS |
|---|---|---|---|---|---|---|
| **Rhodamine B** | 2.92 ns | 2.96 ns | < 8 ns | < 8 ns | n/a | n/a |
| **$Ir(BT)_2(acac)$** | 97 ns | 1.62 µs | 103 ns | > 1 µs | 93 ns (350 nm)<br>112 ns (760nm) | > 400 ns (350 nm)<br>> 500 ns (760nm) |
| **BCC-TPTA** | 6.4 ns | 7.8 ns | 10 ns | 13 ns | n/a | n/a |

***Table S2***. Emissive lifetime and kinetic traces comparison of the investigated chromophores. The emissive lifetimes where done by the TCSPC technique while the kinetic traces were obtained from the ns TAS measurements.

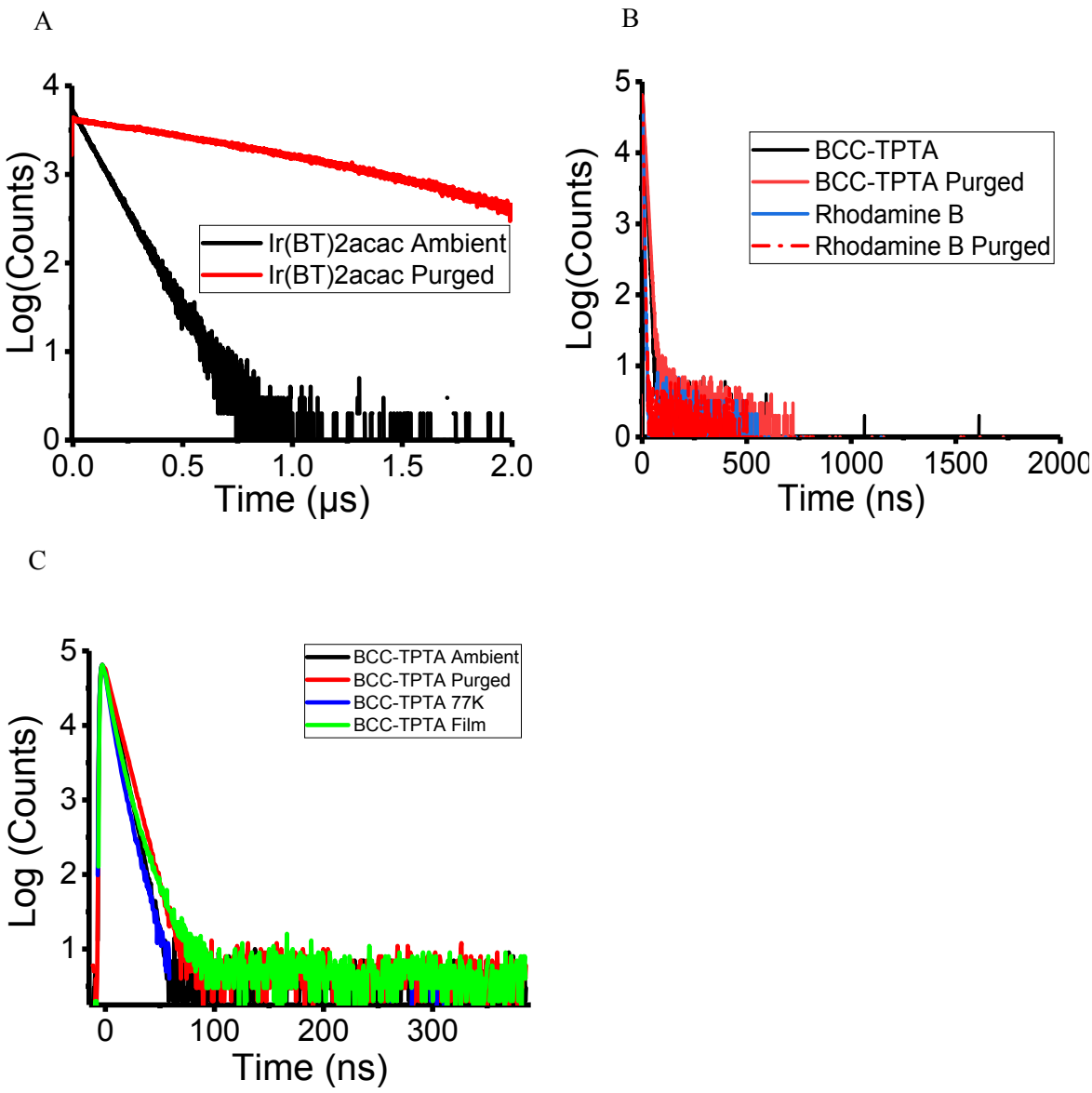


***Figure S10.*** The emissive lifetime of the investigated chromophores probed with the TCSPC technique: $Ir(BT)_2(acac)$ (**A**), BCC-TPTA and Rhodamine B (**B**), BCC-TPTA in PMMA films and 77K (C). In these graphs, a logarithmic approach was taken to plot the data. This allow us to evaluate, if any, small emissive contributions from the triplet-excited state to the delayed fluorescence process. As can be observed, there is a lengthened in the fluorescence lifetime for BCC-TPTA within the first 100 ns after the oxygen purging process. No sign of a delayed fluorescence process was observed for BCC-TPTA after 100 ns before or after the oxygen purging process for BCC-TPTA.

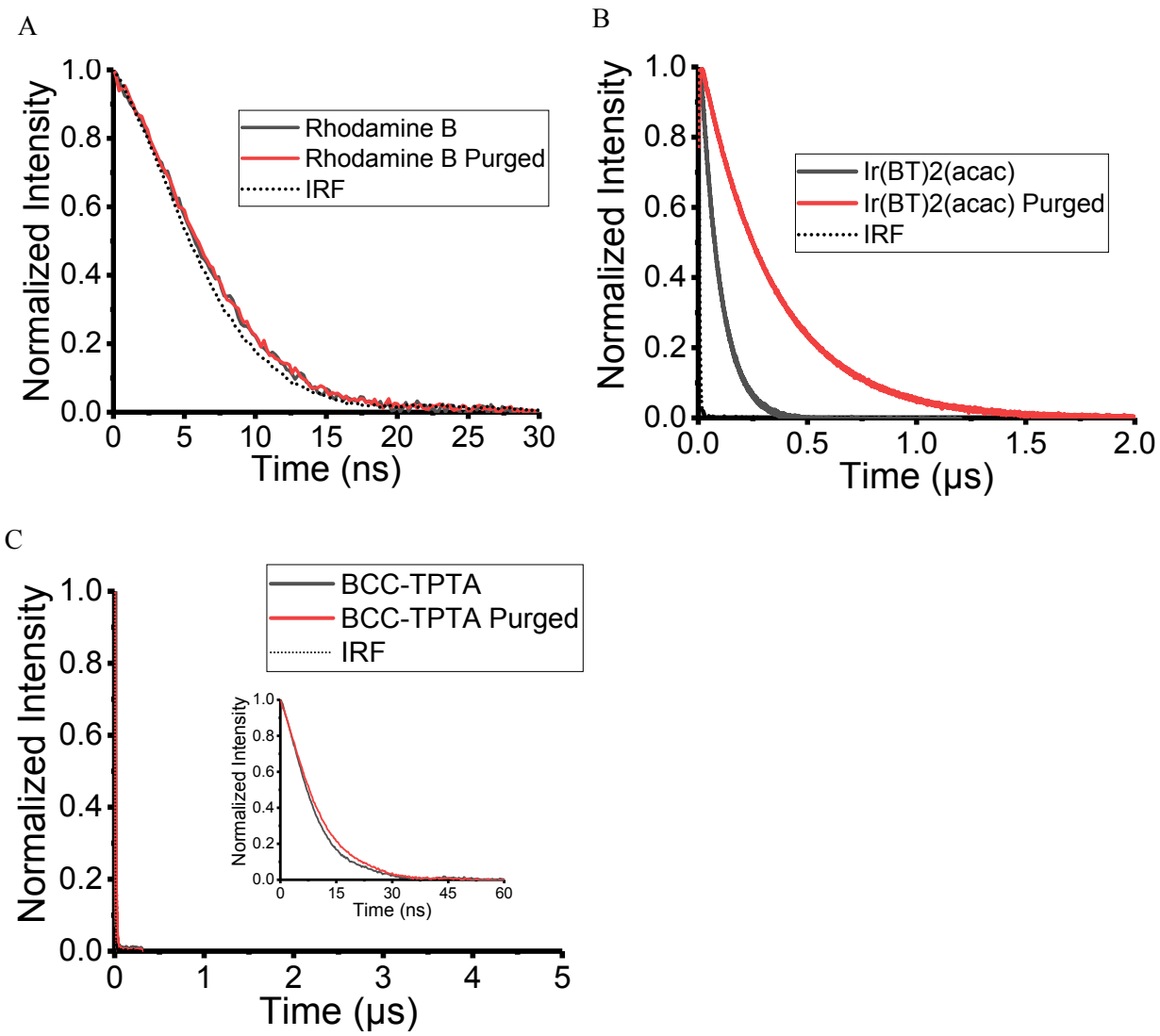


***Figure S11.*** The emissive lifetime of the investigated chromophores probed with the ns TAS technique: Rhodamine B (**A**), Ir(BT)$_2$(acac) (**B**), BCC-TPTA (**C**) in toluene. Inserted in (**C**) is a closed up to the firs 60 ns of the emissive lifetime characterization of BCC-TPTA. The emissive lifetime were also measured after the oxygen purging process and match perfectly with the emissive dynamics probed by using the TCSPC (***Figure 2***).

| Chromophores | Emissive Lifetime | | | | Emissive Lifetime (Purged) | | | |
|---|---|---|---|---|---|---|---|---|
| | $A_1$ | $\tau_1$ (ps) | $A_2$ | $\tau_2$ (ps) | $A_1$ | $\tau_1$ (ps) | $A_2$ | $\tau_2$ (ps) |
| **Rhodamine B** | 0.35 | > 4000 | ~ | ~ | 0.35 | > 4000 | ~ | ~ |
| **Ir(BT)$_2$(acac)** | [a] | [a] | [a] | [a] | [a] | [a] | [a] | [a] |
| **BCC-TPTA** | 0.14 | 27 | 0.65 | 1040 | 0.09 | 21 | 0.68 | 1070 |

***Table S3.*** Emissive lifetime measurements taken with the fluorescence Up-Conversion. [(a)]Not measurable emission decay from this excited state.

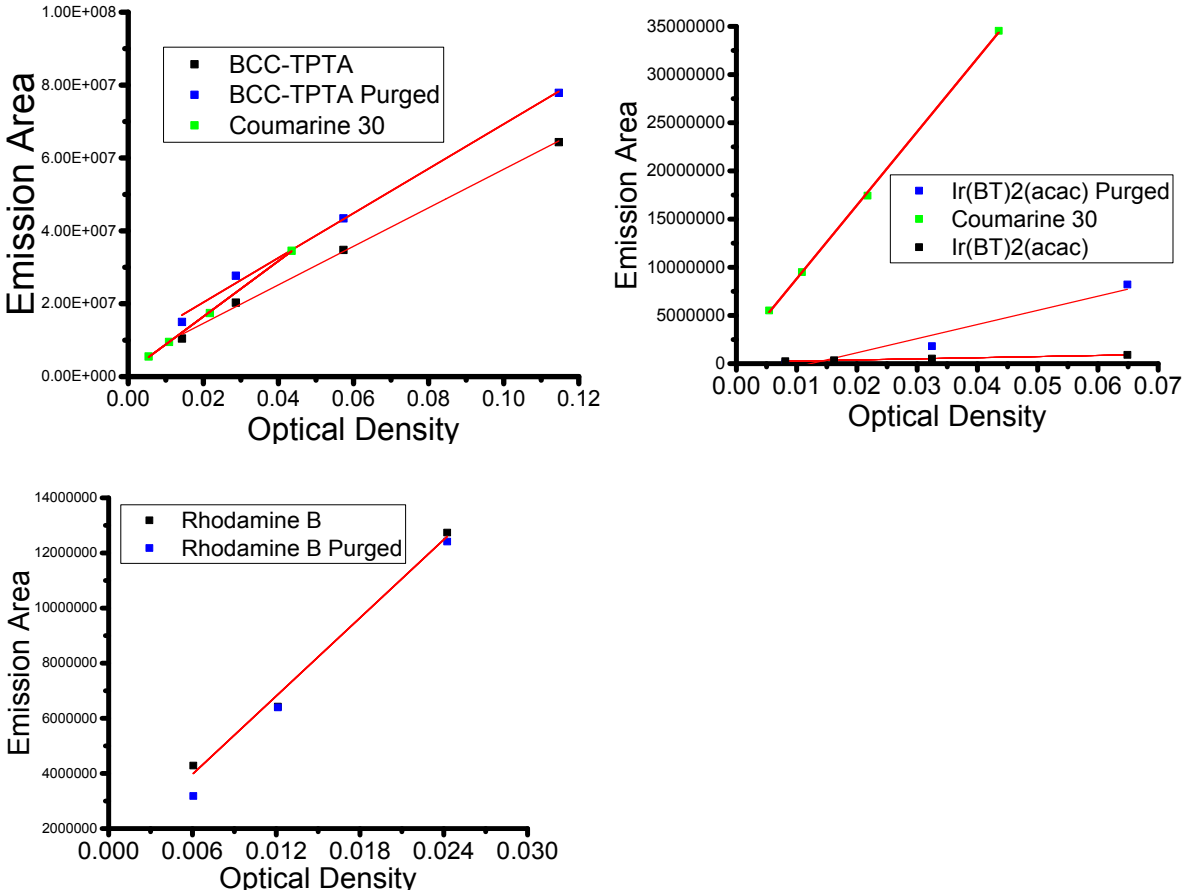


***Figure S12.*** Integrated Area in function of their Optical Density. The slope/gradient of these graph were used for the Quantum Yield calculations.

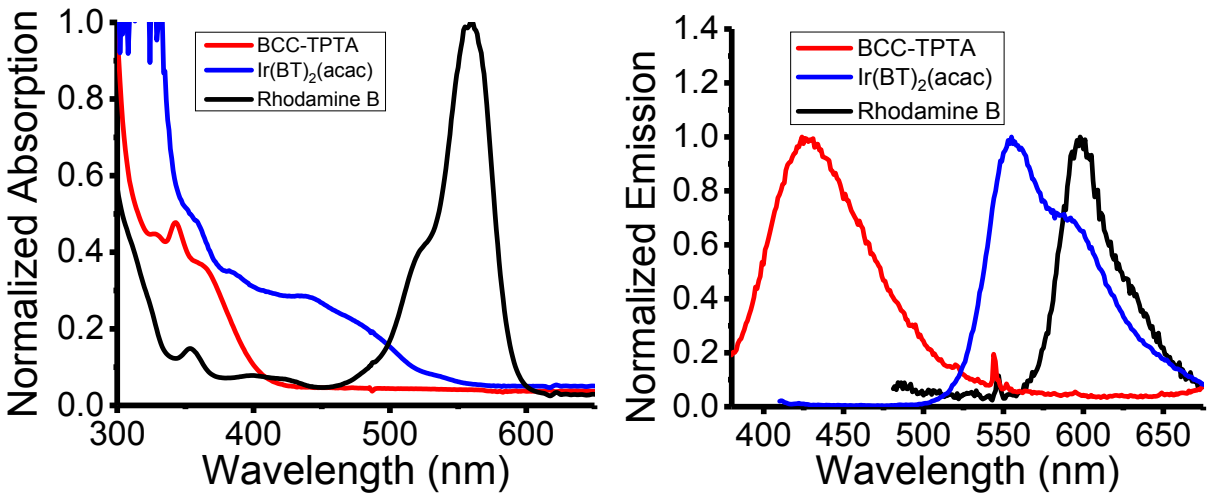


***Figure S13.*** Steady state properties of the investigated chromophores measured in PMMA inert films.

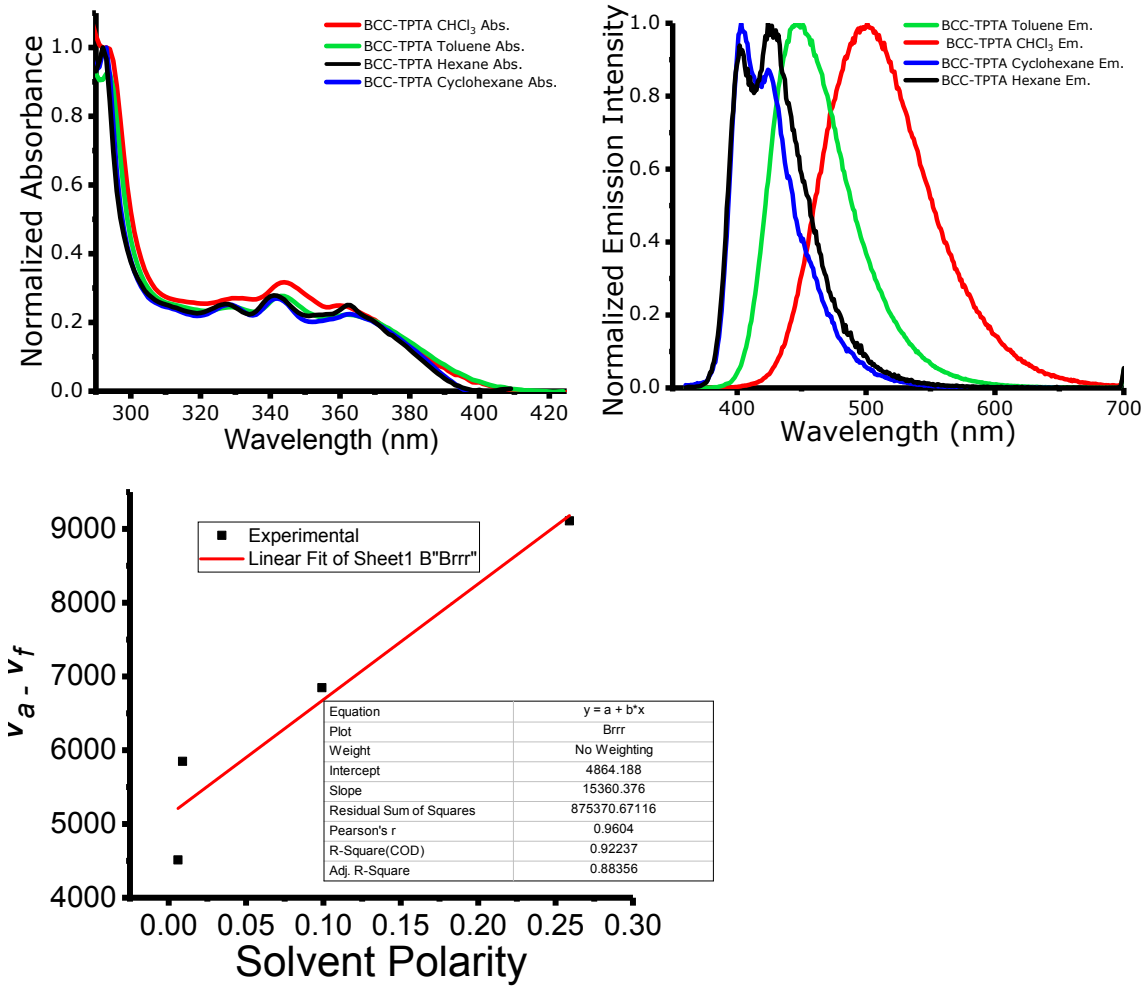


***Figure S14.*** Steady state properties of the investigated chromophores measured in different solvents. From these steady state measurements was extracted the information for the Lippert-Mataga model.

**Quantum Chemical Simulation**

The ground state ($S_0$) geometries of BCC-TPTA and Rhodamine B were optimized using density functional theory (DFT). The B3LYP functional, which has successfully predicted the $\Delta E_{ST}$ of a variety of TADF materials, was used along with the 6-31G* basis set.[6] The first excited singlet state ($S_1$) geometry of BCC-TPTA was obtained with a restricted open-shell Kohn-Sham (ROKS) approach and 6-31G* basis sets. ROKS is known to improve the deficiency of semilocal linear response time-dependent DFT (LR−TD−DFT) and offers a good alternative for investigating charge transfer states.[7–11] Rhodamine B is a symmetric molecule and has a positive unit charge on one nitrogen atom. Due to a closed manifold of low−lying states, however, excited−state geometry optimization of Rhodamine B using TDDFT and ROKS did not easily lead to a symmetry broken state. Therefore, $S_1$ of Rhodamine B was targeted using CIS geometry optimization, which had no issue distinguishing the two states. (B. Carlotti, Z. Cai, H. Kim, V. Sharapov, I. K. Madu, D. Zhao, W. Chen, P. M. Zimmerman, L. Yu, and T. Goodson III, Charge transfer and aggregation effects on the performance of planar vs. twisted non-fullerene acceptor isomers for organic solar cells, Chem. Mater. Under revision) The single point energy of $S_1$ is refined using TD-DFT based on ROKS BCC-TPTA geometry and CIS Rhodamine B geometry.

The first triplet ($T_1$) geometry was predicted with spin−unrestricted DFT. Single point energy calculations to evaluate the fluorescence emission energies, spin−orbit coupling elements, and adiabatic energy gap ($\Delta E_{ST} = E_{\text{TDDFT } S1 \text{ at min } S1} - E_{\text{UDFT } T1 \text{ at min } T1}$) were conducted, and the solvent environment effect is treated using a polarizable continuum model. The dielectric constant of chloroform and ethanol of 4.31 and 24.3 is used to describe the solvent medium of BCC-TPTA solution and Rhodamine B solution, respectively. All quantum chemical calculations were

performed using Q−Chem 5.0.[12] The rate constant of ISC and rISC, were estimated via Fermi's Golden rule,[13,14]

$$k_{ISC} = \frac{2\pi}{\hbar}\rho_{FC}\left|\langle S_1|H_{SO}|T_1\rangle\right|^2$$

where $\langle S_1|H_{SO}|T_1\rangle$ is the spin−orbit coupling element between $S_1$ and $T_1$, $\rho_{FC}$ denotes the Fracnk−Condon−weighted density of states, and $\hbar$ is the reduced Planck constant of $6.582\times10^{-16}$ eVs. $\rho_{FC}$ is evaluated with Marcus−Levich−Jortner theory, [15,16]

$$\rho_{FC} = \frac{1}{\sqrt{4\pi\lambda_M k_B T}}\sum_{n=0}^{\infty}\exp(-S)\frac{S^n}{n!}exp[-\frac{(\Delta E_{ST} + n\hbar\omega_{eff} + \lambda_M)^2}{4\pi\lambda_M k_B T}]$$

where $\lambda_M$ is the Marcus reorganization energy associated with the intermolecular and intramolecular low−frequency vibrations, $k_B$ is for Boltzmann constant of $8.6173\times10^{-5}$ eV/K, T is the temperature (in this study, 298.15 K), $\hbar\omega_{eff}$ represents the effective energy of a mode representing the nonclassical high−frequency intramolecular vibrations. Huang−Rhys factor associated with these modes are given as $S$. The rate constant of the rISC process was described by parameters generated at the $T_1$ geometry, and the $k_{ISC}$ estimation with parameters relevant to the $S_1$ geometry.

One recent computational study on TADF mechanism discussed the rate of rISC within the same framework used in this work. hey computed the contribution of non-classical intramolecular vibrations and estimated the Marcus reorganization energy due to low−frequency intramolecular vibrations and the medium-induced relaxation effects to be in the range of ~0.1-0.2 eV.,[16–18] Also, they assumed the Huang−Rhys factors can be neglected without significant changes to the results for large molecules. The approximation setting $\lambda_M$ to 0.1 or 0.2 eV reproduced available experimental $k_{RISC}$ values on the same order of magnitude. The close examination revealed that

use $\lambda_M$ value of 0.2 eV gave better quantitative agreement with the available experimental $k_{RISC}$ dta. Therefore, $\lambda_M$ value is set to 0.2 eV in this study.

The fluorescence emission rate ($k_F$) was approximated by the product of the oscillator strength and the square of the wavenumber.[19] The observed $k_F$ values of anthraquinone-based intramolecular charge transfer compounds, one class of TADF materials reported by the Adachi's group, could be reproduced with this simple calculation.[19]

*The contribution of $T_2$:* The possibility that ISC and rISC could involve an excited triplet state (higher than $T_1$) was examined based on the vertical triplet energy gap. It is possible for $T_2$ to contribute triplet population transfer if it is energetically close to $T_1$. For BCC-TPTA, $T_2$ is lying 0.42 eV (0.24 eV) above $T_1$ ($S_1$), which indicates the contribution of $T_2$ to both ISC and rISC will be small. Regardless, the rate constants are high, and an additional ISC channel is not needed to account for the significant rate of ISC. Therefore, the contribution of triplet states above $T_1$ can be safely neglected for BCC-TPTA.

The inclusion of $T_2$ in the ISC model for Rhodamine B, however, is significant. The rate constant of ISC between $S_1$ and $T_1$ in this chromophore is small due to the large energy gap (-1.369 eV), which places the transition in the Marcus inverted region, in addition to low spin−orbit coupling (0.053 $cm^{-1}$). The vertical energy difference between $T_1$ and $T_2$ in Rhodamine B is 0.43 eV, and $\Delta E_{ST}$ is reduced to -0.623 eV which acts as driving force for singlet population transfer to $T_2$. $k_{ISC}$ is increased to $1.0\times10^4$ which correlates with the available experimental value to within an acceptable range.

| | $S_1 \rightarrow T_1$ | $S_1 \rightarrow T_2$ | $S_1 \rightarrow T_n$ Expt.[a] |
|---|---|---|---|
| **Spin−orbit coupling ($cm^{-1}$)** | 0.053 | 0.381 | N/A |
| **$\Delta E_{ST}$ (eV)** | -1.369 | -0.623 | N/A |
| **$k_{ISC}$ ($s^{-1}$)** | $2.3\times10^{-23}$ | $1.4\times10^{4}$ | $5.3\times10^{5}$ |

***Table S4.*** Spin−orbit coupling, energy gap between $S_1$ and $T_n$ ($\Delta E_{ST}$), and rate constant of ISC process in Rhodamine B. [(a)] Results in ethylene glycol. Chem. Phys. Lett., 1998, 291, 237.

References


(1) Jones, G.; Jackson, W. R.; Choi, C. Y.; Bergmark, W. R. Solvent Effects on Emission Yield and Lifetime for Coumarin Laser Dyes. Requirements for a Rotatory Decay Mechanism. *J. Phys. Chem.* **1985**, *89*, 294–300.

(2) Beaumont, P. C.; Johnson, D. G.; Parsons, B. J. Photophysical Properties of Laser Dyes: Picosecond Laser Flash Photolysis Studies of Rhodamine 6G, Rhodamine B and Rhodamine 101. *J. Chem. Soc. Faraday Trans.* **1993**, *89*, 4185.

(3) Lakowicz, J. R.; Weber, G. Quenching of Fluorescence by Oxygen. a Probe for Structural Fluctuations in Macromolecules. *Biochemistry* **1973**, *12*, 4161–4170.

(4) Schweitzer, C.; Schmidt, R. Physical Mechanisms of Generation and Deactivation of Singlet Oxygen. *Chem. Rev.* **2003**, *103*, 1685–1758.

(5) Ware, W. R. Oxygen Quenching of Fluorescence in Solution: An Experimental Study of the Diffusion Process. *J. Phys. Chem.* **1962**, *66*, 455–458.

(6) Hirata, S.; Sakai, Y.; Masui, K.; Tanaka, H.; Lee, S. Y.; Nomura, H.; Nakamura, N.; Yasumatsu, M.; Nakanotani, H.; Zhang, Q.; et al. Highly Efficient Blue Electroluminescence Based on Thermally Activated Delayed Fluorescence. *Nat. Mater.* **2015**, *14*, 330–336.

(7) Kowalczyk, T.; Tsuchimochi, T.; Chen, P. T.; Top, L.; Van Voorhis, T. Excitation Energies and Stokes Shifts from a Restricted Open-Shell Kohn-Sham Approach. *J. Chem. Phys.* **2013**, *138*, 164101.

(8) Hait, D.; Zhu, T.; McMahon, D. P.; Van Voorhis, T. Prediction of Excited-State Energies and Singlet-Triplet Gaps of Charge-Transfer States Using a Restricted Open-Shell Kohn-Sham Approach. *J. Chem. Theory Comput.* **2016**, *12*, 3353–3359.

(9) Frank, I.; Hutter, J.; Marx, D.; Parrinello, M. Molecular Dynamics in Low-Spin Excited States. *J. Chem. Phys.* **1998**, *108*, 4060–4069.

(10) Okazaki, I.; Sato, F.; Yoshihiro, T.; Ueno, T.; Kashiwagi, H. Development of a Restricted

Open Shell Kohn-Sham Program and Its Application to a Model Heme Complex. *J. Mol. Struct. THEOCHEM* **1998**, *451*, 109–119.

(11) Filatov, M.; Shaik, S. A Spin-Restricted Ensemble-Referenced Kohn–Sham Method and Its Application to Diradicaloid Situations. *Chem. Phys. Lett.* **1999**, *304*, 429–437.

(12) Shao, Y.; Gan, Z.; Epifanovsky, E.; Gilbert, A. T. B.; Wormit, M.; Kussmann, J.; Lange, A. W.; Behn, A.; Deng, J.; Feng, X.; et al. Advances in Molecular Quantum Chemistry Contained in the Q-Chem 4 Program Package. *Mol. Phys.* **2015**, *113*, 184–215.

(13) Robinson, G. W.; Frosch, R. P. Electronic Excitation Transfer and Relaxation. *J. Chem. Phys.* **1963**, *38*, 1187–1203.

(14) Lawetz, V.; Orlandi, G.; Siebrand, W. Theory of Intersystem Crossing in Aromatic Hydrocarbons. *J. Chem. Phys.* **1972**, *56*, 4058–4072.

(15) Brédas, J.-L.; Beljonne, D.; Coropceanu, V.; Cornil, J. Charge-Transfer and Energy-Transfer Processes in π-Conjugated Oligomers and Polymers: A Molecular Picture. *Chem. Rev.* **2004**, *104*, 4971–5004.

(16) Schmidt, K.; Brovelli, S.; Coropceanu, V.; Beljonne, D.; Cornil, J.; Bazzini, C.; Caronna, T.; Tubino, R.; Meinardi, F.; Shuai, Z.; et al. Intersystem Crossing Processes in Nonplanar Aromatic Heterocyclic Molecules. *J. Phys. Chem. A* **2007**, *111*, 10490–10499.

(17) Beljonne, D.; Shuai, Z.; Pourtois, G.; Bredas, J. L. Spin-Orbit Coupling and Intersystem Crossing in Conjugated Polymers: A Configuration Interaction Description. *J. Phys. Chem. A* **2001**, *105*, 3899–3907.

(18) Samanta, P. K.; Kim, D.; Coropceanu, V.; Brédas, J. L. Up-Conversion Intersystem Crossing Rates in Organic Emitters for Thermally Activated Delayed Fluorescence: Impact of the Nature of Singlet vs Triplet Excited States. *J. Am. Chem. Soc.* **2017**, *139*, 4042–4051.

(19) Zhang, Q.; Kuwabara, H.; Potscavage, W. J.; Huang, S.; Hatae, Y.; Shibata, T.; Adachi, C. Anthraquinone-Based Intramolecular Charge-Transfer Compounds: Computational Molecular Design, Thermally Activated Delayed Fluorescence, and Highly Efficient Red Electroluminescence. *J. Am. Chem. Soc.* **2014**, *136*, 18070–18081.